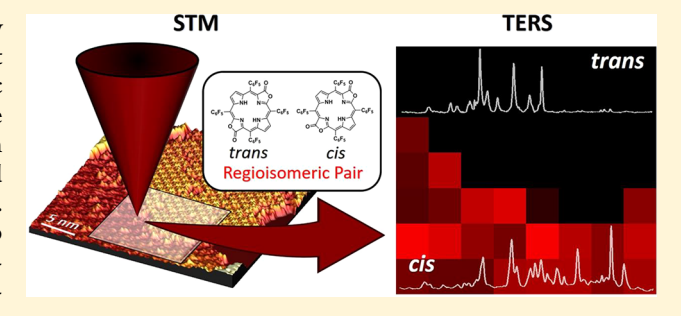
Downloaded via UNIV OF ILLINOIS CHICAGO on May 10, 2019 at 22:19:35 (UTC). See https://pubs.acs.org/sharingguidelines for options on how to legitimately share published articles.

Angstrom Scale Chemical Analysis of Metal Supported Trans- and Cis-Regioisomers by Ultrahigh Vacuum Tip-Enhanced Raman **Mapping**

Sayantan Mahapatra, Yingying Ning, Jeremy F. Schultz, Linfei Li, Jun-Long Zhang, Jeremy F. Schultz, Linfei Li, and Nan Jiang*,†®

Supporting Information

ABSTRACT: Real space chemical analysis of two structurally very similar components, that is, regioisomers lies at the heart of heterogeneous catalysis reactions, modern-age electronic devices, and various other surface related problems in surface science and nanotechnology. One of the big challenges in surface chemistry is to identify different surface adsorbed molecules and analyze their chemical properties individually. Herein, we report a topological and chemical analysis of two regioisomers, trans- and cis-tetrakispentafluorophenylporphodilactone (trans- and cis-H₂F₂₀TPPDL) molecules by highresolution scanning tunneling microscopy, and ultrahigh



vacuum tip-enhanced Raman spectroscopy (UHV-TERS). Both isomeric structures are investigated individually on Ag(100) at liquid nitrogen temperature. Following that, we have successfully distinguished these two regioisomeric molecules simultaneously through TERS with an angstrom scale (8 Å) spatial resolution. Also, the two-component organic heterojunction has been characterized at large scale using high-resolution two-dimensional mapping. Combined with time-dependent density functional theory simulations, we explain the TERS spectral discrepancies for both isomers in the fingerprint region.

KEYWORDS: Angstrom scale, regioisomer, ultrahigh vacuum scanning tunneling microscopy (UHV-STM), single molecule spectroscopy, tip-enhanced Raman spectroscopy (TERS), time-dependent density functional theory (TDDFT)

he study and characterization of regioisomeric molecules 👤 (positional isomers) on a surface in real space has immense importance in the fields of nanotechnology, surface chemistry, heterogeneous catalysis, molecular electronics, and so forth. For instance, in regioselective catalysis reactions performed on metal surfaces such as the dehydrogenation of alkyl species, C=C bond migration, and cis-trans isomerization in olefins, two or more regioisomers can be obtained as products. 1-3 Specification of these regioisomeric products at the single molecular level holds broad and diverse applications towards controlling these reactions. On the other hand, elucidating two-component organic heterostructure systems is critical to understanding and manipulating the properties of many modern electronic devices such as gate-tunable p-n diodes, donor-acceptor charge transfer, and so forth. While many techniques are capable of characterizing surface admolecules, few of them can provide molecular level information with high accuracy and precision. Scanning probe techniques such as scanning tunneling microscopy (STM) can image a self-assembled monolayer of any flat molecules with submolecular resolution. However, STM cannot distinguish regioisomeric molecules as they hold very

similar electronic structure. Therefore, it is necessary to probe the vibrational properties of the surface-bound molecules and interrogate the chemical information at the angstrom scale.^{6–10}

Tip-enhanced Raman spectroscopy (TERS) emerges as a special approach which provides the topographic images of single molecules using metallic tips and chemical identification through Raman spectroscopy.^{7,11–16} Plasmonic metal probes were used to not only detect tunneling current from the surface as in STM but also to probe and access the vibrational modes with an impressive spatial resolution. 6,8,17-21 Remarkable progresses have been achieved in applying TERS in the characterization of carbon nanotubes, ²², ²³ biomolecules, ^{24–29} two-dimensional (2D) materials, ^{30,31} monitoring catalytic processes, 32-35 and so forth. In particular, TERS imaging was used to successfully detect a dynamic molecular phase boundary³⁶ and nanodefects in 2D covalent monolayers.³⁷ Using TERS mapping, it is possible to distinguish adjacent porphyrin molecules on Ag(111)³⁸ and metastable surface-

Received: February 25, 2019 Revised: April 15, 2019 Published: April 17, 2019

Department of Chemistry, University of Illinois at Chicago, Chicago, Illinois 60607, United States

[‡]Beijing National Laboratory for Molecular Sciences, College of Chemistry and Molecular Engineering, Peking University, Beijing 100871, P.R. China

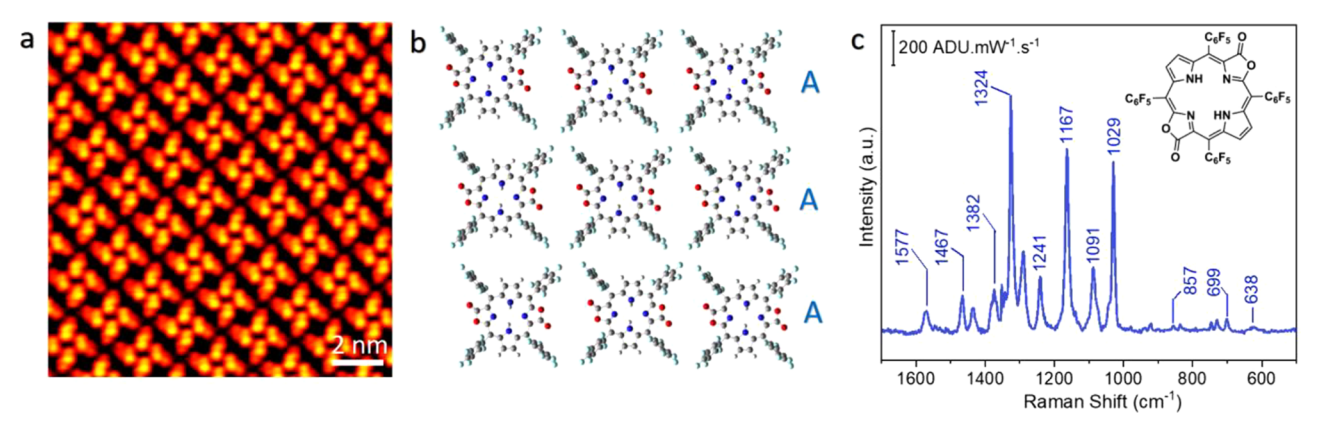


Figure 1. STM and TERS study of trans- H_2F_{20} TPPDL on Ag(100). (a) STM topograph of trans-isomer (V = -1.2 V, I = 150 pA). (b) Tentative model for trans molecular self-assembly indicates "AAA"-type packing. (c) TERS fingerprint for the trans- H_2F_{20} TPPDL on Ag(100). Tip-retracted signal is subtracted from the tip-engaged signal. $\lambda_{ex} = 633$ nm, $P_{acq} = 0.5$ mW, $t_{acq} = 10$ s, six accumulations. Tip-engaged, tip-retracted spectra are highlighted in the Supporting Information (Figure S2). (Inset) Chemical structure of trans- H_2F_{20} TPPDL.

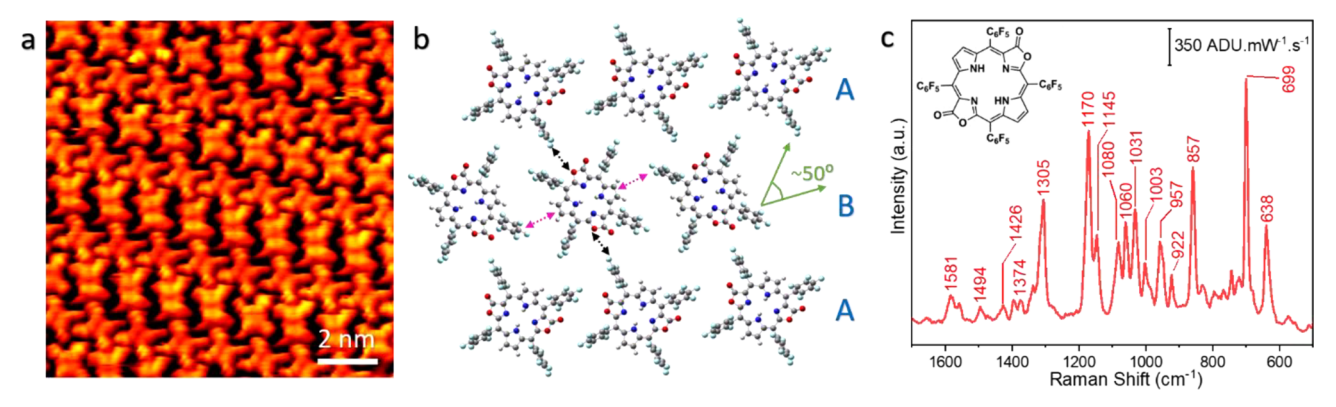


Figure 2. STM and TERS study of cis- H_2F_{20} TPPDL on Ag(100). (a) STM topograph of cis-isomer (V = -1.5 V, I = 150 pA). (b) A tentative model of cis molecular self-assembly indicates "ABA"-type packing where row B rotates from row A by ~50°. The interactions involving pyrrole rings (with lactone moieties) with adjacent phenyl ($-C_6F_5$) rings are indicated by dotted black double headed arrows, whereas for the other two pyrrole rings (no lactone moieties) they are indicated by dotted pink double headed arrows. (c) TERS fingerprint of cis- H_2F_{20} TPPDL on Ag(100). Tip-retracted signal is subtracted from the tip-engaged signal. $\lambda_{\rm ex} = 633$ nm, $P_{\rm acq} = 0.5$ mW, $t_{\rm acq} = 10$ s, six accumulations. Tip-engaged and tip-retracted spectra are highlighted in the Supporting Information (Figure S4). (Inset) Chemical structure of cis- H_2F_{20} TPPDL.

mediated conformations of porphyrin derivatives on Cu(111) with angstrom scale resolution.³⁹ However, using TERS to study the regioisomeric effect of molecules has never been reported.

Regioisomeric effect in porphodilactone (PDL), where two opposite pyrrole rings of porphyrin are oxidized to lactone moieties, plays important roles in modulating the photophysical properties of porphyrins.⁴⁰ Switching the carbonyl groups from cis- to trans-isomer leads to 19 nm red shift of the $Q_{\nu}(0,0)$ band, mimicking the regioisomeric effect in natural chlorophyll b, d, and f. 40 The relative orientation of the lactone moieties was also found to finely modulate their function in triplet-triplet annihilation, singlet oxygen, and lanthanide sensitization. $^{40-42}$ In this letter, we demonstrate a topographic analysis using UHV-STM and an angstrom scale resolution chemical identification through TERS to investigate the regioisomeric effect in trans- and cis-tetrakispentafluorophenylporphodilactone 40 (trans- and cis-H₂F₂₀TPPDL) and manage to distinguish them precisely on an atomically pristine single crystal Ag(100) surface. Even though they are isomers, alternating the lactone moieties causes a slight change in their electronic structure which is reflected in their vibrational fingerprint data. By combining time-dependent density functional theory (TDDFT) calculations, we can accurately distinguish these two chemical structurally similar components by applying a TERS line profile (8 $\mbox{\normalfont\AA}$ resolution) and 2D imaging.

The Ag(100) single crystal (Princeton Scientific, 99.999% purity) was cleaned by repeated cycles of Argon ion sputtering (1 kV, $\sim 2.5 \times 10^{-5}$ Torr), followed by annealing at ~ 800 K. trans- and cis-H₂F₂₀TPPDL molecules, synthesized and purified according to literature, 40 were deposited on the clean Ag(100) surface in a submonolayer coverage using a molecular evaporator held at ~500 K in UHV. After that, the samples were transferred to the STM chamber for further STM and TERS experiments, which were performed at liquid nitrogen temperature (~77 K). The plasmonically active Ag tip (electrochemically etched) was cleaned in UHV by argon ion sputtering (1.5 kV, \sim 2.5 \times 10⁻⁵ Torr) and used for STM and TERS experiments. TERS signals were acquired with excitation of a 633 nm continuous wave (cw) HeNe (LASOS) laser and detected by an iso-plane SCT320 spectrograph (Princeton Instrument) coupled with a Princeton Instrument PIXIS 100 CCD. Detailed experimental setup can be found in our previous publication.⁴³ We performed pre-resonance Raman calculations (633 nm) at the S₀ optimized crystal structure with hybrid density functional, B3LYP, 44,45 using the

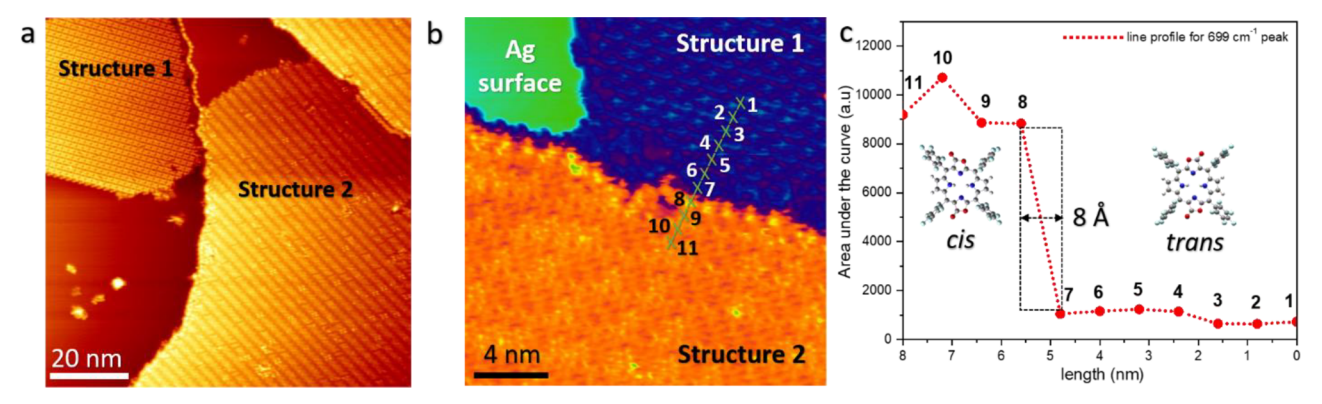


Figure 3. Angstrom scale TERS analysis of codeposited *trans*- and *cis*-porphodilactone molecules on Ag(100). (a) STM topographic image (100 nm \times 100 nm) of codeposited *trans*- and *cis*-isomers where Structure 1 and Structure 2 were identified. (V = -1.65 V, I = 150 pA). (b) Zoom-in STM image (V = -1.50 V, I = 150 pA) where we performed the TERS line profile measurements. Eleven points are marked by green crosses. Also, Structure 1 (blue), Structure 2 (orange), and the bare Ag surface (green) are highlighted. (c) TERS line profile measured with Ag tip for 699 cm⁻¹ peak (area under the curve) with spatial resolution 8 Å. $\lambda_{\rm ex} = 633$ nm, $P_{\rm acq} = 0.5$ mW, $t_{\rm acq} = 10$ s at each point.

program package Gaussian 09 (Revision E.01).⁴⁶ The 6-31G(d) basis set was used for all atoms.^{47,48}

We first investigated the trans-porphodilactone isomers using STM after they were deposited on Ag(100) when the substrate was held at room temperature. The STM image, as shown in Figure 1a, reveals a typical "pinwheel" conformation, ⁴⁹⁻⁵¹ which is slightly different compared to the gas phase structure where the phenyl $(-C_6F_5)$ rings remain perpendicular with respect to the porphyrin core. They form a "regular" arrangement where the individual molecules can be clearly seen (Figure 1a). Figure 1b shows a tentative model of this molecular self-assembly in which the molecules are arranged in "AAA"-type packing. A 633 nm incident laser irradiation has been introduced to interrogate their vibrational properties as it is close to the actual excited electronic state $[Q_{\nu}(0,0)]$ of the molecule (Figure S1). Figure 1c represents the TERS signature of trans-H₂F₂₀TPPDL molecules while the tip is scanning over molecular islands. We labeled most of the peaks in the TERS spectrum in which a dominant peak was observed at 1324 cm⁻¹ along with few other modes in the fingerprint region.

Following that, we deposited the cis-H₂F₂₀TPPDL molecules with similar coverage on clean Ag(100). In comparison with the trans, the cis-isomers also took a "pinwheel" conformation while the packing in the self-assembly appears to be completely distinct, as shown in Figure 2a. The different orientation of the lactone moieties in the cis-isomers introduces a "zig-zag" pattern where the molecular rows are now packed in "ABA"type fashion, as displayed in Figure 2b. Considering the fact that only two opposite pyrrole rings possess the lactone moieties, they can interact with the adjacent phenyl $(-C_6F_5)$ groups of other cis molecules in mainly two different ways which are denoted by dotted black and pink double headed arrows in Figure 2b. On the basis of this argument, we propose another tentative model for this arrangement in Supporting Information (Figure S3) which arises from slightly different interactions. The proposed model shows that the molecules from row B are rotated either $\sim 50^{\circ}$ (Figure 2b) or $\sim 130^{\circ}$ (Figure S3) compared to the molecules from row A. Figure 2c depicts the TERS fingerprint for cis-H₂F₂₀TPPDL molecules on Ag(100). Contrary to trans-isomers, significantly strong and intense peak features were discovered for the cis-isomers in the lower wavenumber region (500-900 cm⁻¹). We will discuss the reason later. Such spectral intensity differences in this region enables us to distinguish them in real space.

The growing interest of multicomponent films is of great importance to address lots of questions ranging from modern electronic devices and systems⁴ to donor-acceptor charge transfer.⁵ Different types of organic structures can either selfrecognize themselves, establish separate self-assemblies,³⁸ diffuse on the substrates at room temperature thus initiating mixed and irregular molecular 2D networks.⁵² For some applications, one may require random distribution of one component in another⁵³ whereas in other cases internal ordering seems desirable. 52 If these components hold very similar electronic structure, for example, different metalloporphyrins,⁵⁴ alone STM is inadequate to capture the complete picture. So, it is of great interest to chemically identify these distinct but electronically similar components at well-defined interfaces. Therefore, to study the two-component organic heterostructure system, we sequentially deposited both trans- and cis-H₂F₂₀TPPDL on Ag(100) when the sample was held at room temperature. Figure 3a shows a large domain picture (100 nm × 100 nm) of their molecular self-assemblies in which they were found mainly in extensive, large islands. Two different self-assembled structural forms were identified. The left-hand side of the image (Figure 3a) where the island appears relatively clear is defined as Structure 1, and the righthand side where the islands are noisy (line like pattern) is identified as Structure 2. The observation of the two selfassembled structural forms is independent of which component is deposited first. These two self-assemblies may be limited to either cis- or trans-isomers or can be a mixed structural form composed of both. Because of the deposition of structurally similar skeletons (regioisomers), distinguishing them on the surface is now beyond the capacity of STM. At this point, it is quite reasonable to probe their vibrational properties by TERS. Changing the orientation of lactone moieties can alter their vibrational properties which is evident from their Raman fingerprint data.

Figure 3b shows a zoom-in STM image where we conducted the TERS line profile experiment. Structure 1 and Structure 2 were highlighted using blue and orange color, respectively. To identify the molecules directly from the undefined self-assembled structure, we performed sequential TERS measurements across the line as shown in Figure 3b. A total 8 nm length was chosen by taking 11 points which were distributed across one structural form to the other. In other words, from points 1–7, the tip was kept on Structure 1, whereas for the

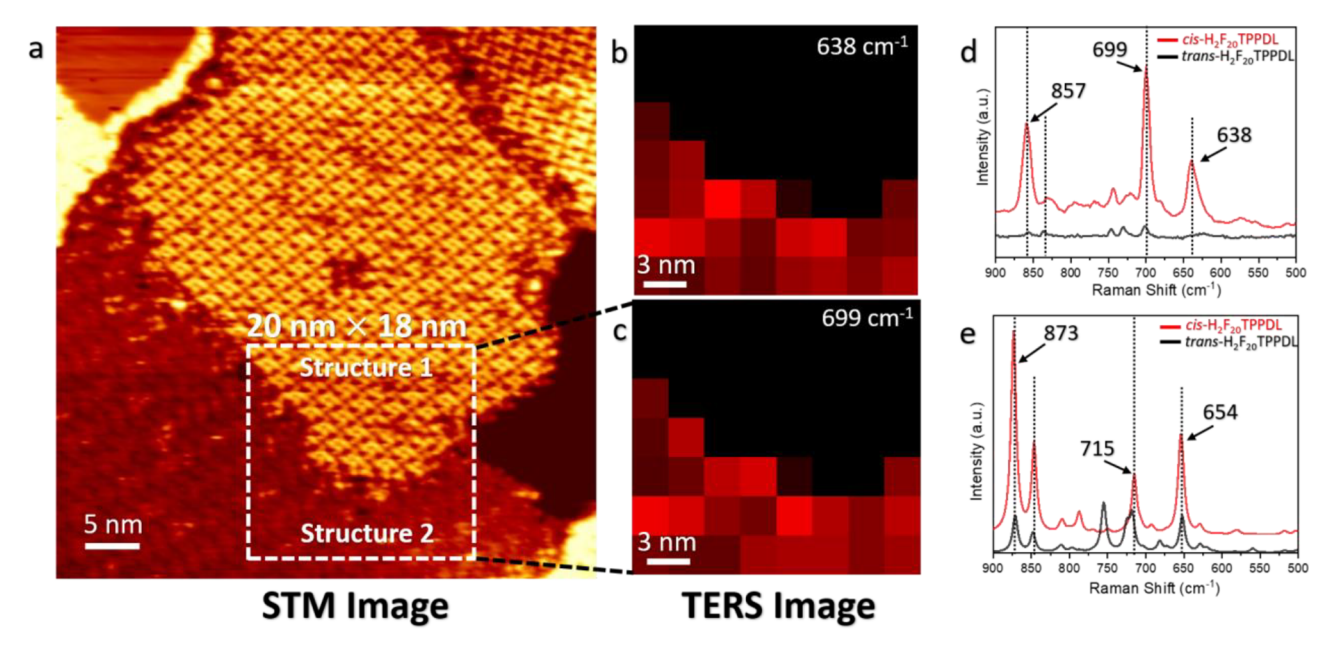


Figure 4. TERS 2D mapping of co-deposited regioisomeric molecules on Ag(100). (a) STM image of coadsorbed *trans*- and *cis*-isomers (V = -1.46 V, I = 150 pA). A white dotted rectangle area (20 nm \times 18 nm) was selected to obtain the TERS images where Structure 1 and Structure 2 were identified. (b,c) TERS images by tracking 638 and 699 cm⁻¹ peaks, respectively (8 pixels \times 7 pixels). $\lambda_{\rm ex} = 633 \text{ nm}$, $P_{\rm acq} = 0.5 \text{ mW}$, 2.5 nm step size per pixel, $t_{\rm acq} = 10 \text{ s}$ at each pixel. (d) Comparison of experimental TERS spectra (tip-retracted signal is subtracted from the tip-engaged signal) of cis- (red) and trans-isomers (black) in the 500–900 cm⁻¹ region where 638, 699, and 857 cm⁻¹ peaks were identified. (e) TDDFT-simulated spectra obtained from pre-resonance Raman (633 nm) calculations for *cis*- (red) and *trans*-isomers (black), 654, 715, and 873 cm⁻¹ peaks were marked.

remaining 4 points, that is, for points 8-11, we moved the tip to the Structure 2 molecular island. The tip was held at each point for 10 s to acquire the TERS spectra. In the low wavenumber region (500-900 cm⁻¹), the realization of weak TERS intensities were verified for the first 7 points (1-7)while relatively pronounced, intense peak features were obtained for the last 4 points (8-11). Figure 3c represents the line profile of the strongest peak (699 cm⁻¹) observed in this concerned region with angstrom scale (8 Å) resolution. This spatial resolution allows us to chemically distinguish the trans-H₂F₂₀TPPDL from its adjacent cis-H₂F₂₀TPPDL, as the length of both the isomers is ~1.3 nm (Figure S1), therefore confirming each TERS signal originates from an individual, single molecule adsorbed on the surface. With this single molecule sensitivity, we were able to confirm roughly four molecules from Structure 1 (along the points 1-7) are only trans-porphodilactone isomers while about three molecules from Structure 2 (along the points 8-11) island are only cisporphodilactone isomers. We also observe fluctuations in the line profile (Figure 3c), for example, from the 3rd to 4th point or from the 9th to 10th point, which can be attributed to the fact that TERS signal can vary with different tip positions over a single molecule.³⁸ This result demonstrates that TERS provides accurate chemical identification of surface-adsorbed individual molecules and provides new opportunities to investigate regioselective catalysis reactions at the angstrom scale.

Integrating different organic structures with relevant electronic properties into the lateral 2D heterostructures, linked through weak van der Waals interactions, offers exciting properties at the heterojunction. Therefore, to understand how the *trans*- and *cis*-isomers fabricate into the self-assembled network and visualize the two-component organic heterojunction at the nanometer scale, we need to perform TERS 2D

mapping in our system. To explore the large domain picture, we now keep the distance between the points (acquiring the TERS spectra) fixed at 2.5 nm (step size) for 2D mapping. Figure 4a describes a large-scale STM picture of two coexisting self-assembled molecular islands in which Structure 1 and Structure 2 were identified for clarification. Figure 4b,c reveals high-resolution TERS images collected from a 20 nm \times 18 nm area, indicated by a white-dotted rectangle in Figure 4a. Because of the difference in intensities at the 500-900 cm⁻¹ region, three strong peaks (active for cis but almost silent for trans) at 638, 699, and 857 cm⁻¹ were chosen and tracked to construct the Raman images (detailed data analysis can be found in Supporting Information, Figure S5). Figure 4b,c represents the TERS images for 638 and 699 cm⁻¹ peaks, respectively, whereas the mapping figure for the 857 cm⁻¹ peak is presented in Supporting Information (Figure S6). The pixels from the molecule-molecule domain boundary (heteromolecular junction) show excellent contrast change (Figure 4b, c) in their profile. In Supporting Information, we also introduced two raw TERS spectra from the mapping zone, one from Structure 1 and another from Structure 2 molecular islands, to compare with the original TERS spectra (tip-engaged) of transand cis-isomers that were already acquired (Figure S6). The fingerprints, that is, peak positions and intensities match with each other for both the spectra. Our analysis confirms the molecules detected from the Structure 1 island are all trans-H₂F₂₀TPPDL, whereas those on the Structure 2 island are all cis-H₂F₂₀TPPDL. As in this two-component system, these two regioisomers can self-recognize themselves, and they independently form separate ordered self-assembled structure within their van der Waals contact. Therefore, we ruled out the possibility of having random distribution of one structure in another,⁵⁴ phase change,³⁶ or loss of ordering⁵⁶ in our system.

We also interpreted our TERS results with pre-resonance Raman (633 nm) TDDFT simulations of individual gas phase trans- and cis-H₂F₂₀TPPDL molecules. Figure 4d describes a relative comparison of TERS spectra for cis- and trans-isomers in the 500-900 cm⁻¹ region whereas the simulated Raman spectra are shown in Figure 4e. We found significant similarities between the simulated (TDDFT) spectra and experimentally observed TERS spectra which reveals strong, intense vibrational modes for cis-isomers but not for transisomers, identifying relatively weak peaks in the concerned region (500-900 cm⁻¹). Also, a shift in the peak positions (14-16 cm⁻¹) was identified for the experimental TERS spectra (638, 699, and 857 cm⁻¹) compared to simulation (654, 715, and 873 cm⁻¹, Figure S7), which is consistent for both the trans- and cis-isomers and can be explained in terms of molecule-molecule⁵⁷ and molecule-substrate³⁸ interactions. As discussed earlier, the molecular packing can be considerably altered from trans to cis isomers and different wavenumber peak shifts were expected to be observed for trans- and cisisomers separately. However, the same value-peak position shifting for both trans- and cis-isomers (as shown using black dotted lines Figure 4d) suggests that the intermolecular interactions are not strong enough to perturb the vibrational modes in this case. On the other hand, these two isomers hold very similar structural skeleton, hence molecule-substrate interaction can be comparable for both. The slight mismatch in peak position between the experimental TERS spectra and simulated Raman spectra can be explained by the interactions between the molecules and Ag(100) substrate which could be responsible for charge transfer between the molecule and substrate. Note that the observed intensity mismatch in the spectra between theory and experiment could be justified by the fact that the $Q_{\nu}(0,0)$ band is in a different position for both of the isomers compared to the excitation laser (Figure S1). Therefore, we conclude that the TDDFT simulation confirms the intensity discrepancies between cis- and trans-isomers in the 500-900 cm⁻¹ region whereas the molecule-substrate interaction leads to a shift in the Raman modes compared to simulations.

In conclusion, using an STM combined-TERS system we have demonstrated the regioisomeric effect of this new class of porphyrinoids, that is, porphodilactones (PDL) at interfaces and shown a new method to distinguish these very similar structural forms simultaneously with high accuracy and precision. Trans- and cis-porphodilactone isomers are involved in the formation of separate, independently-ordered selforganized assemblies, as seen in the high-resolution Raman (TERS) images. Our findings are consistent with TDDFT simulations that show a higher intensity in the Raman spectrum for cis- in comparison with trans-isomers in the low wavenumber region. The fact that the regioisomeric molecules can be distinguished, as demonstrated here, indicates enormous advancements in heterogeneous catalysis field. Furthermore, resolving the organic 2D heteromolecular domain boundary in a two-component system, that is, interfacial interactions between the ordered self-assembled layers play important roles in the performance of molecular electronic devices. We anticipate this work will provide significant insight into single molecule studies in a range of fields, such as the characterization of chemical and catalytic reactions, and also demonstrate a potential analytical technique to understand the chemical properties of lateral 2D

heterojunctions, involving organic, semiconductor, or different 2D materials with subnanometer precision.

ASSOCIATED CONTENT

S Supporting Information

The Supporting Information is available free of charge on the ACS Publications website at DOI: 10.1021/acs.nanolett.9b00826.

Ball and stick model of *trans*-H₂F₂₀TPPDL and absorbance spectra of *trans*- and *cis*-isomers; TERS spectra of the *trans*-H₂F₂₀TPPDL (tip engaged and tip withdrawn); proposed model for *cis*-H₂F₂₀TPPDL self-assembly; TERS spectra of *cis*-H₂F₂₀TPPDL (tip engaged and tip withdrawn); data analysis for TERS mapping; Comparison between raw TERS spectra from mapping and original TERS fingerprint for *trans*- and *cis*-isomers; TDDFT simulated vibrational modes for *cis*-H₂F₂₀TPPDL (PDF)

AUTHOR INFORMATION

Corresponding Authors

*E-mail: njiang@uic.edu.

*E-mail: zhangjunlong@pku.edu.cn.

ORCID 4

Jeremy F. Schultz: 0000-0003-2231-6797 Jun-Long Zhang: 0000-0002-5731-7354 Nan Jiang: 0000-0002-4570-180X

Notes

The authors declare no competing financial interest.

ACKNOWLEDGMENTS

N.J. acknowledges support from startup funding of the University of Illinois at Chicago. J.F.S. and N.J. acknowledge support from the National Science Foundation (CHE-1807465). Acknowledgement is made to the donors of the ACS Petroleum Research Fund for partial support of this research. J.-L. Z. acknowledges financial support from National Scientific Foundation of China (NO. 21778002, 21621061 and 21861162008).

REFERENCES

- (1) Lee, I.; Zaera, F. J. Am. Chem. Soc. 2005, 127 (35), 12174–12175.
- (2) Morales, R.; Zaera, F. J. Phys. Chem. B 2006, 110 (19), 9650-9659.
- (3) Lewis, E. A.; Marcinkowski, M. D.; Murphy, C. J.; Liriano, M. L.; Therrien, A. J.; Pronschinske, A.; Sykes, E. C. H. *Chem. Commun.* **2017**, *53* (55), *7816–7819*.
- (4) Dhar, B. M.; Kini, G. S.; Xia, G.; Jung, B. J.; Markovic, N.; Katz, H. E. *Proc. Natl. Acad. Sci. U. S. A.* **2010**, *107* (9), 3972–3976.
- (5) Fernández-Torrente, I.; Franke, K. J.; Pascual, J. I. *Phys. Rev. Lett.* **2008**, *101* (21), 217203.
- (6) Pozzi, E. A.; Goubert, G.; Chiang, N.; Jiang, N.; Chapman, C. T.; McAnally, M. O.; Henry, A.-I.; Seideman, T.; Schatz, G. C.; Hersam, M. C.; Duyne, R. P. V. Chem. Rev. 2017, 117 (7), 4961–4982.
- (7) Stöckle, R. M.; Suh, Y. D.; Deckert, V.; Zenobi, R. Chem. Phys. Lett. 2000, 318 (1), 131-136.
- (8) Verma, P. Chem. Rev. 2017, 117 (9), 6447-6466.
- (9) Deckert-Gaudig, T.; Taguchi, A.; Kawata, S.; Deckert, V. Chem. Soc. Rev. 2017, 46 (13), 4077–4110.
- (10) Lee, J.; Tallarida, N.; Chen, X.; Jensen, L.; Apkarian, V. A. Sci. Adv. 2018, 4 (6), No. eaat5472.
- (11) Anderson, M. S. Appl. Phys. Lett. 2000, 76 (21), 3130-3132.

(12) Chiang, N.; Jiang, N.; Chulhai, D. V.; Pozzi, E. A.; Hersam, M. C.; Jensen, L.; Seideman, T.; Van Duyne, R. P. *Nano Lett.* **2015**, *15* (6), 4114–4120.

- (13) Pettinger, B.; Ren, B.; Picardi, G.; Schuster, R.; Ertl, G. Phys. Rev. Lett. 2004, 92 (9), 096101.
- (14) Park, K.-D.; Muller, E. A.; Kravtsov, V.; Sass, P. M.; Dreyer, J.; Atkin, J. M.; Raschke, M. B. *Nano Lett.* **2016**, *16* (1), 479–487.
- (15) Sonntag, M. D.; Klingsporn, J. M.; Garibay, L. K.; Roberts, J. M.; Dieringer, J. A.; Seideman, T.; Scheidt, K. A.; Jensen, L.; Schatz, G. C.; Van Duyne, R. P. J. Phys. Chem. C 2012, 116 (1), 478–483.
- (16) Su, H.-S.; Zhang, X.-G.; Sun, J.-J.; Jin, X.; Wu, D.-Y.; Lian, X.-B.; Zhong, J.-H.; Ren, B. Angew. Chem., Int. Ed. **2018**, 57 (40), 13177–13181.
- (17) Jiang, N.; Foley, E. T.; Klingsporn, J. M.; Sonntag, M. D.; Valley, N. A.; Dieringer, J. A.; Seideman, T.; Schatz, G. C.; Hersam, M. C.; Van Duyne, R. P. *Nano Lett.* **2012**, *12* (10), 5061–5067.
- (18) Tallarida, N.; Rios, L.; Apkarian, V. A.; Lee, J. Nano Lett. 2015, 15 (10), 6386-6394.
- (19) Zhang, R.; Zhang, Y.; Dong, Z. C.; Jiang, S.; Zhang, C.; Chen, L. G.; Zhang, L.; Liao, Y.; Aizpurua, J.; Luo, Y.; Yang, J. L.; Hou, J. G. Nature 2013, 498, 82.
- (20) Lee, J.; Tallarida, N.; Chen, X.; Liu, P.; Jensen, L.; Apkarian, V. A. ACS Nano 2017, 11 (11), 11466-11474.
- (21) Zhang, R.; Zhang, X.; Wang, H.; Zhang, Y.; Jiang, S.; Hu, C.; Zhang, Y.; Luo, Y.; Dong, Z. Angew. Chem., Int. Ed. 2017, 56 (20), 5561–5564.
- (22) Anderson, N.; Hartschuh, A.; Cronin, S.; Novotny, L. J. Am. Chem. Soc. 2005, 127 (8), 2533–2537.
- (23) Chen, C.; Hayazawa, N.; Kawata, S. Nat. Commun. 2014, 5, 3312.
- (24) Bailo, E.; Deckert, V. Angew. Chem., Int. Ed. 2008, 47 (9), 1658-1661.
- (25) Domke, K. F.; Zhang, D.; Pettinger, B. J. Am. Chem. Soc. 2007, 129 (21), 6708–6709.
- (26) Lipiec, E.; Sekine, R.; Bielecki, J.; Kwiatek, W. M.; Wood, B. R. Angew. Chem., Int. Ed. **2014**, 53 (1), 169–172.
- (27) Najjar, S.; Talaga, D.; Schué, L.; Coffinier, Y.; Szunerits, S.; Boukherroub, R.; Servant, L.; Rodriguez, V.; Bonhommeau, S. J. Phys. Chem. C 2014, 118 (2), 1174–1181.
- (28) Xiao, L.; Schultz, Z. D. Cancer Cell Microenviron 2016, 3 (4), No. e1419.
- (29) Wang, H.; Schultz, Z. D. ChemPhysChem 2014, 15 (18), 3944–3949.
- (30) Beams, R.; Vamivakas, A. N.; et al. *Nanotechnology* **2015**, *26* (17), 175702.
- (31) Sheng, S.; Wu, J.-b.; Cong, X.; Li, W.; Gou, J.; Zhong, Q.; Cheng, P.; Tan, P.-h.; Chen, L.; Wu, K. *Phys. Rev. Lett.* **2017**, *119* (19), 196803.
- (32) Nguyen, D.; Kang, G.; Chiang, N.; Chen, X.; Seideman, T.; Hersam, M. C.; Schatz, G. C.; Van Duyne, R. P. *J. Am. Chem. Soc.* **2018**, *140* (18), 5948–5954.
- (33) van Schrojenstein Lantman, E. M.; Deckert-Gaudig, T.; Mank, A. J. G.; Deckert, V.; Weckhuysen, B. M. Nat. Nanotechnol. 2012, 7, 583.
- (34) Kazuma, E.; Jung, J.; Ueba, H.; Trenary, M.; Kim, Y. Science **2018**, 360 (6388), 521.
- (35) Zhong, J.-H.; Jin, X.; Meng, L.; Wang, X.; Su, H.-S.; Yang, Z.-L.; Williams, C. T.; Ren, B. *Nat. Nanotechnol.* **2016**, *12*, 132.
- (36) Jiang, N.; Chiang, N.; Madison, L. R.; Pozzi, E. A.; Wasielewski, M. R.; Seideman, T.; Ratner, M. A.; Hersam, M. C.; Schatz, G. C.; Van Duyne, R. P. *Nano Lett.* **2016**, *16* (6), 3898–3904.
- (37) Shao, F.; Dai, W.; Zhang, Y.; Zhang, W.; Schlüter, A. D.; Zenobi, R. ACS Nano 2018, 12 (5), 5021–5029.
- (38) Jiang, S.; Zhang, Y.; Zhang, R.; Hu, C.; Liao, M.; Luo, Y.; Yang, J.; Dong, Z.; Hou, J. G. Nat. Nanotechnol. 2015, 10, 865.
- (39) Chiang, N.; Chen, X.; Goubert, G.; Chulhai, D. V.; Chen, X.; Pozzi, E. A.; Jiang, N.; Hersam, M. C.; Seideman, T.; Jensen, L.; Van Duyne, R. P. *Nano Lett.* **2016**, *16* (12), 7774–7778.

(40) Ke, X. S.; Chang, Y.; Chen, J. Z.; Tian, J.; Mack, J.; Cheng, X.; Shen, Z.; Zhang, J. L. J. Am. Chem. Soc. 2014, 136 (27), 9598–9607.

- (41) Ke, X. S.; Ning, Y.; Tang, J.; Hu, J. Y.; Yin, H. Y.; Wang, G. X.; Yang, Z. S.; Jie, J.; Liu, K.; Meng, Z. S.; Zhang, Z.; Su, H.; Shu, C.; Zhang, J. L. Chem. Eur. J. 2016, 22 (28), 9676–9686.
- (42) Ning, Y.; Ke, X. S.; Hu, J. Y.; Liu, Y. W.; Ma, F.; Sun, H. L.; Zhang, J. L. *Inorg. Chem.* **2017**, *56* (4), 1897–1905.
- (43) Whiteman, P. J.; Schultz, J. F.; Porach, Z. D.; Chen, H.; Jiang, N. J. Phys. Chem. C 2018, 122 (10), 5489-5495.
- (44) Becke, A. D. J. Chem. Phys. 1993, 98 (7), 5648-5652.
- (45) Lee, C.; Yang, W.; Parr, R. G. Phys. Rev. B: Condens. Matter Mater. Phys. 1988, 37 (2), 785-789.
- (46) Frisch, M. J.; Trucks, G. W.; Schlegel, H. B.; Scuseria, G. E.; Robb, M. A.; Cheeseman, J. R.; Scalmani, G.; Barone, V.; Mennucci, B.; Petersson, G. A. et al. *Gaussian 09*, Revision D.01.; Wallingford, CT, 2009.
- (47) Francl, M. M.; Pietro, W. J.; Hehre, W. J.; Binkley, J. S.; Gordon, M. S.; DeFrees, D. J.; Pople, J. A. J. Chem. Phys. **1982**, 77 (7), 3654–3665.
- (48) Hariharan, P. C.; Pople, J. A. Theor. Chim. Acta 1973, 28 (3), 213-222.
- (49) Rojas, G.; Chen, X.; Bravo, C.; Kim, J.-H.; Kim, J.-S.; Xiao, J.; Dowben, P. A.; Gao, Y.; Zeng, X. C.; Choe, W.; Enders, A. *J. Phys. Chem. C* **2010**, *114* (20), 9408–9415.
- (50) Auwärter, W.; Écija, D.; Klappenberger, F.; Barth, J. V. Nat. Chem. 2015, 7, 105.
- (51) Brede, J.; et al. Nanotechnology 2009, 20 (27), 275602.
- (52) Gottfried, J. M. Surf. Sci. Rep. 2015, 70 (3), 259-379.
- (53) Ramachandran, G. K.; Hopson, T. J.; Rawlett, A. M.; Nagahara, L. A.; Primak, A.; Lindsay, S. M. Science 2003, 300 (5624), 1413.
- (54) Scudiero, L.; Barlow, D. E.; Hipps, K. W. J. Phys. Chem. B 2000, 104 (50), 11899–11905.
- (55) Lee, G.-H.; Lee, C.-H.; van der Zande, A. M.; Han, M.; Cui, X.; Arefe, G.; Nuckolls, C.; Heinz, T. F.; Hone, J.; Kim, P. APL Mater. **2014**, 2 (9), 092511.
- (56) Barlow, D. E.; Scudiero, L.; Hipps, K. W. Langmuir **2004**, 20 (11), 4413-4421.
- (57) Chiang, N.; Jiang, N.; Madison, L. R.; Pozzi, E. A.; Wasielewski, M. R.; Ratner, M. A.; Hersam, M. C.; Seideman, T.; Schatz, G. C.; Van Duyne, R. P. *J. Am. Chem. Soc.* **2017**, *139* (51), 18664–18669.